Engineering Topological Surface States: HgS, HgSe, and HgTe

François Virot,[1,2] Roland Hayn,[1,*] Manuel Richter,[3] and Jeroen van den Brink[3]

[1]*CNRS, Aix-Marseille Université, IM2NP-UMR 7334, 13397 Marseille Cedex 20, France*

[2]*Centre de Cadarache, Institut de Radioprotection et de Sûreté Nucléaire, PSN-RES/SAG/LETR, 13115 Saint Paul les Durance Cedex, France*

[3]*IFW Dresden, Helmholtzstraße 20, 01069 Dresden, Germany*

(Received 27 February 2013; published 2 October 2013)

Using density functional electronic structure calculations, we establish the consequences of surface termination and modification on protected surface states of metacinnabar (β-HgS). Whereas we find that the Dirac cone is isotropic and well separated from the valence band for the (110) surface, it is highly anisotropic at the pure (001) surface. We demonstrate that the anisotropy is modified by surface passivation because the topological surface states include contributions from dangling bonds. Such dangling bonds exist on all pure surfaces within the whole class HgX with X = S, Se, or Te and directly affect the properties of the Dirac cone. Surface modifications also alter the spatial location (depth and decay length) of the topologically protected edge states, which renders them essential for the interpretation of photoemission data.

DOI: 10.1103/PhysRevLett.111.146803 PACS numbers: 73.20.−r, 72.80.Sk

An attractive perspective for spintronics was opened up by the discovery [1–3] and manufacturing [4–6] of topological insulators (TIs). Inside, in its bulk, a TI is insulating but on its boundary—the material's edges, surfaces, or interfaces—a TI is conducting. The first TI in which the topological character of its edge states was established is HgTe, a mercury chalcogenide material of the HgX family (where X = S, Se, Te) with a zincblende crystal structure [4]. The understanding of the precise properties of the topological edge states in the HgX family of TIs—and an understanding of how these can be altered and engineered—is of fundamental importance in the field. It is of course also of direct relevance to the development of future spintronics applications, which aims to exploit the spin-momentum locking of TI boundary electrons [7,8] allowing, for instance, the generation of edge-spin-currents by circularly polarized light [9–11]. The precise location and electronic structure of the topological surface states, in particular their dispersion, play furthermore an essential role in determining their spin-transport characteristics. It is, for instance, well known that the momentum-spin locking usually renders disordered TIs poor spin conductors: when the electronic spin is tied to its momentum each scattering event randomizes the spin [12,13]. It was recently established that the resulting limit on the spin relaxation time τ_S for edge-state electrons strongly depends on their dispersion and momentum space anisotropy [14].

Here we show that for the HgX class of mercury-based II-VI semiconductors in the zincblende structure there is a strong influence of existing dangling bonds on the properties of topological surface states. Thus, by surface passivation, it is possible to achieve a strong modification of the spatial location of the topological states, their rate of decay into the bulk, the resulting Dirac cone dispersion, and, in particular, the Dirac cone anisotropy. Such alterations are possible because the presence of topological edge states is absolutely fixed by the topological invariants of the bulk electronic structure, but the shape of their dispersion, their location with respect to the surface, and their orbital character are not. On the (001) surface, decoration has an immediate effect on the Dirac cone dispersion and anisotropy, which we will demonstrate in detail for HgX (001) surfaces where hydrogen passivates the dangling bonds. A comparison between HgS (001) and (110) surfaces reveals that the location and anisotropy of the topological states also strongly depend on the surface type.

Bulk HgTe is an inverted gapless semiconductor, since the Fermi level is located in the fourfold degenerate Γ_8 level. A tetragonal distortion is needed to open a gap, thus converting HgTe into a three-dimensional TI [15]. HgSe is believed to be similar to HgTe as it has an inverted band structure [16] with Γ_6 lying below Γ_8. In contrast, in metacinnabar (β-HgS) the twofold degenerate Γ_7 level lies above Γ_8 and presumably forms the bottom of the conduction band [17], which is however still a subject of debate. Some theoretical investigations found this material at ambient pressure to be a standard semiconductor with the s-like Γ_6 state in the conduction band [16,18] while others confirm that it is an inverted semiconductor [19–21]. It should be noted that the conclusions that we will present here on the surface states and their anisotropy are independent of how such debates are settled. We focus on the HgX compounds to illustrate the principle of topological surface state engineering by the controlled chemical and crystallographic modification of these states which should be applicable to TIs in general.

To this end we performed density functional based electronic structure calculations using the all-electron,

full potential local orbital method [22,23] on HgX slabs with and without surface passivation. All calculations were done in the local density approximation [24], where the presented band structures and projected eigenstates were evaluated in a four-component relativistic mode, while self-consistency was achieved in a scalar-relativistic mode. The valence basis set is comprised of the states Hg ($5s$, $5p$, $5d$, $6s$, $6p$, $6d$, $7s$), S ($2s$, $2p$, $3s$, $3p$, $3d$, $4s$, $4p$), Se ($3s$, $3p$, $3d$, $4s$, $4p$, $4d$, $5s$, $5p$), Te ($4s$, $4p$, $4d$, $5s$, $5p$, $5d$, $6s$, $6p$), and H ($1s$, $2s$, $2p$).

In order to model the surfaces, we consider stacks of $(\mathrm{Hg}X)_4$ cells, spaced by an empty (vacuum) layer of $16.5 \cdots 25.8$ Å thickness. Mercury termination is assumed for all (001) surfaces since we found this termination to be most stable in agreement with the experimental observations on HgTe [25] and HgSe [26]. To satisfy the stoichiometry, every second Hg atom has to be removed from the (001) surfaces giving rise to a $c(2 \times 2)$ reconstruction, which was observed on HgSe [26] and HgTe [25]. We have considered in addition a decoration of these $c(2 \times 2)$ (001) surfaces by two H atoms per surface cell, which are placed on top of the surface Hg atoms and in the voids (see Fig. 1). In these calculations we relaxed the z positions of the decorating H atoms. For HgS (001), the cells in the stack are cubic with an experimental lattice constant $a = 5.85$ Å. For (001) stacks of HgSe and HgTe we used tetragonally distorted cells, $a \neq c$, with a gap at the Γ point. All (001) slabs have tetragonal symmetry (space group 111). To build the (110) HgS slab, we used an orthorhombic cell (space group 25 with the stack in the x direction) and the same atomic distances as for the (001) slab. Contrary to (001), the (110) surface is stoichiometric without any reconstruction. The $\mathbf{k}$-space integrations were carried out using the linear tetrahedron method with Blöchl corrections and $8 \times 8 \times 1/4 \times 4 \times 1$ points in the full Brillouin zone for (001) and (110) slabs.

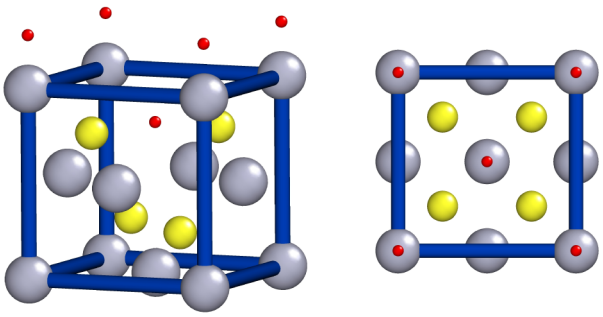

FIG. 1 (color online). Conventional elementary cell of HgX with decorated surface. Left panel: perspective view. Right panel: top view onto the (001) surface. Each $(\mathrm{Hg}X)_4$ cell in the interior of the stack consists of four atomic layers as shown in the lower part of the cell (Hg, large gray spheres; X, medium yellow spheres). At the Hg-terminated surface, every second atom is removed. H atoms (small red spheres) are added in some of the calculations to saturate the dangling bonds.

We first discuss results of bulk calculations for tetragonally strained HgSe and HgTe. Since in cubic HgSe and HgTe there is no gap because only two of the four Γ_8 levels are occupied, we consider a strain induced by a CdX (X = Se, Te) substrate. The in-plane lattice constants equal those of the substrate: $a = 6.052$ Å (6.48 Å) for X = Se (Te). In the perpendicular direction, $c = 6.13$ Å (6.45 Å) was calculated [27] using elastic moduli from Ref. [28]. Consequently at the Γ point direct gaps open of 24 and 10 meV for HgSe and HgTe, respectively. This value for HgTe is very close to the measured direct gap of 11 meV [29]. There is also a small indirect gap of 5 meV for HgSe at the considered distortion, but HgTe turns out to be metallic in our calculation in contrast to the recent observation of an indirect gap of 6 meV [29].

Cubic β-HgS was recently predicted to be a strong TI with very anisotropic Dirac cones on the pure $c(2 \times 2)$ (001) surface [21] (cf. the middle panel of Fig. 2). The anisotropy shows up between the two pairs of occupied or unoccupied bands at the Fermi level along the direction Γ-M. One band of each pair belongs to the top, the other to the bottom of the slab, which has no mirror plane parallel to the surface. Both bands are interchanged if the $\mathbf{k}$ direction is rotated by $\pi/2$.

To investigate the influence of the growth direction on the protected surface states, we calculated the electronic structure of the HgS-(110) surface, which is besides (001) another common surface of the zincblende structure [30]. We increased the slab thickness until the residual gap, which is due to the interaction of states at the two opposite surfaces, almost completely closed. A stack of nine cells, 74.45 Å thick, yields a gap of 2.7 meV at Γ. The corresponding band structure is shown in the left panel of Fig. 2, where it is superimposed onto the projected bulk bands. As in the case of the (001) surface, the projected bulk band structure has a direct gap of 42 meV. However, there are two remarkable differences between the topological surface states of the (110) and the (001) surfaces. First, the bands cross almost in the center of the bulk gap for (110), while the (001) surface states cross only slightly above the valence band. Second and most intriguing, the strong anisotropy close to the Dirac point observed for the (001) surface has almost completely vanished in the (110) case. This is shown here for the directions Γ-Y and Γ-T. An almost identical dispersion is found along Γ-Z (not shown). Note, that there is a mirror plane (glide plane for even number of atomic layers) parallel to the surface present in the (110) slab, in contrast to (001). Thus, the top or bottom pairs of states are split only by the residual interaction through the finite slab. The anisotropy is now visible in a (marginal) difference between Γ-Y and Γ-T.

It should be noted that in both cases (001) and (110) there is only a twofold rotational symmetry present at the surface in contrast to the fourfold rotoinversion symmetry of the bulk. Thus, a certain anisotropy of the Dirac cones is

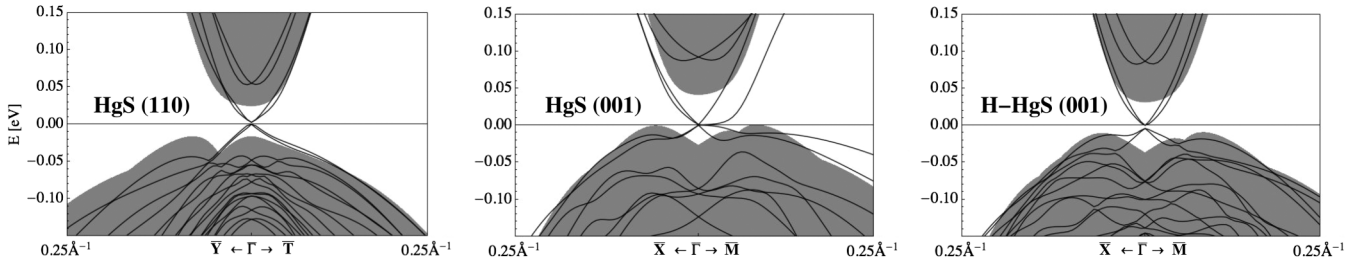

FIG. 2. Left panel: band structure of a nine-cell (110) HgS slab (lines) close to the Γ point along two specific directions, superimposed to the HgS bulk band structure (gray area) projected to the (110) surface. Middle panel: the same for an eight-cell (001) HgS slab (same data as published in Ref. [21]). Right panel: the same for a 12-cell H-passivated HgS slab.

to be expected also for the (110) surface. There, however, each atom is threefold coordinated with bonds forming a regular tripod. The related local threefold axes stick out of the surface plane at an angle of 54.7°. In contrast, chains of bonds dominate the local symmetry at the (001) surface, providing a much stronger second-order ligand field as it is present in the (110) case.

Next, we compare the band structures of (001) HgX slabs with clean surfaces, X = S, Se, Te, shown in the upper row of Fig. 3. As a generic feature, eight states with small dispersion are found in the bulk gap for all three systems. The upper, unoccupied four states are separated from the bulk continuum in the whole **k** space, while the lower states partly merge with the continuum states. By analysis of the atomic contributions (size of red dots in Fig. 3) we assign these eight states to dangling bonds, which appear as remainders, if covalent bonds are cut at a surface. On the (001) surface of HgX, both mercury bonds and bonds involving p orbitals from the first X subsurface layer are broken. These dangling bonds of the Hg-terminated (001) surface give rise to dispersionless surface bands [31,32]. The Dirac cones emerging from the dangling bonds were found to be strongly anisotropic for HgS [21] (see the middle panel of Fig. 2). HgSe (see the middle panel of the upper row in Fig. 3) has a very similar overall electronic structure but no distinct Dirac cone for the present slab thickness due to the much smaller bulk gap. As mentioned before, HgTe is a bulk metal in our calculation. Using a 10 times larger uniaxial strain which safely opens a finite gap, Dirac cones were obtained on differently terminated (001) surfaces of HgTe by applying the *ab initio* based method of maximally localized Wannier functions in Ref. [33]. On the Hg-terminated surface, Dirac points with very small velocities were found at $\bar{X}$ and $\bar{M}$ [33]. This finding we confirm in a calculation for the case of realistic strain (see the upper right panel of Fig. 3).

Next, we consider the effect of surface passivation by addition of hydrogen on the electronic structure of the (001) surfaces. Relaxation of the respective z coordinates of H (see Fig. 1) yields a position 0.24 Å (0.27 Å, 0.31 Å)

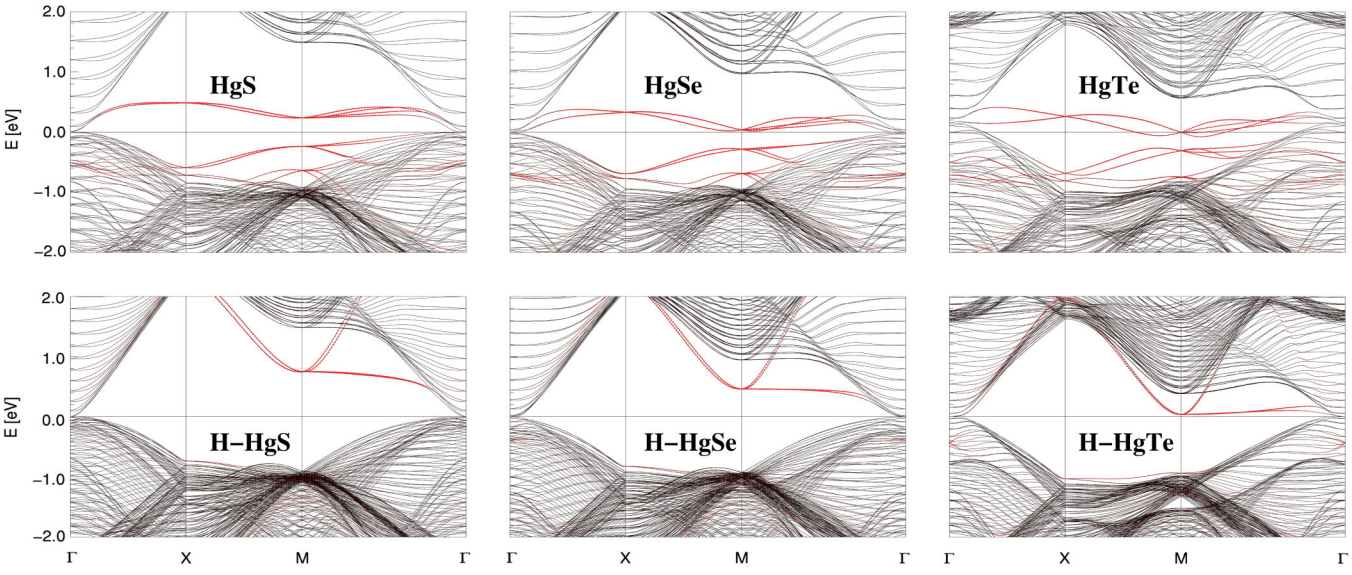

FIG. 3 (color online). Band structures of (001) HgX slabs with zincblende structure. Upper row: stacks of eight cells with clean surfaces. Lower row: stacks of 12 cells with surfaces passivated by hydrogen. From the left to the right, results for β-HgS, HgSe, and HgTe are shown. The size of the red dots on the bands indicates the band weight projected to the outermost HgX_2(H-HgX_2) layers.

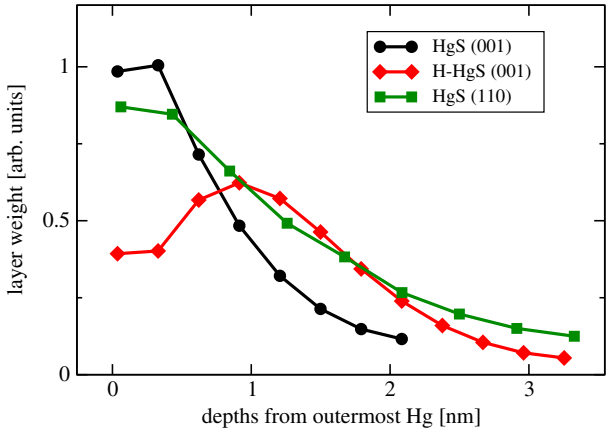

FIG. 4 (color online). Layer-resolved weights of the topological surface states at Γ. The orbital weights are summed over all four states (top and bottom of the slab) and over one HgS atomic double layer [$(HgS)_2$ for (110)]. In the case of H-passivated HgS, the H weights are included in the surface double layer.

above the subsurface sulfur (Se, Te) layer for the hydrogen in the void and a distance of 1.65 Å (1.66 Å, 1.67 Å) between the other hydrogen and the mercury atom underneath. The resulting dispersions are shown in the lower row of Fig. 3. Comparison with the band structure of pristine surfaces in the upper row reveals a considerable reconstruction of the surface states (red dots). In particular, the passivation strongly enhances the dispersion of these states in a bigger part of the **k** space and shifts them away from the Fermi level. We attribute this to the covalency introduced by the H decoration.

The effect of passivation on the Dirac cones is very clearly illustrated by the case of HgS (001), shown in the middle and right panels of Fig. 2 and the left column of Fig. 3. The two bands corresponding to the two surfaces of the slab are nearly degenerate after passivation—the anisotropy of the Dirac cone has virtually disappeared. To understand this effect we calculated the weight contributed by each HgS layer to the surface states, which build the Dirac cone (see Fig. 4). For a clean (001) surface, the topological state is predominantly formed by the dangling bonds and thus located at the outermost atomic layers with a decay length of about 1 nm. (Note, however, that the decay length of the dangling-bond states away from the Dirac point, indicated by large red dots in Fig. 3, is smaller than one atomic double layer of 0.3 nm.) For the passivated surface, however, the maximum weight comes from layers 1 nm underneath the surface (see Fig. 4). There, the crystal potential is already bulklike and the influence of the lower symmetry at the surface is marginal. This explains the very small anisotropy of the Dirac cone. We assign the change of weight distribution to the strong covalency introduced by the passivating hydrogen. For the (110) surface, where less dangling bonds exist than at (001), we find an intermediate situation with the weight maximum at the surface but about a 2 nm decay length. A concomitant effect of the inward shift of the weight, compared with pristine HgS (001), lies in a stronger interaction between top and bottom surface bands. Therefore, the slab thickness had to be increased in the two other systems before a reasonable approximation to a Dirac point was obtained. We note that the type of information contained in Fig. 4 is essential for the understanding of photoemission experiments on TI surface states, since the electron escape depth is limited.

The electronic structures of passivated HgSe and HgTe are very similar to that of H-HgS (see the middle and right columns of Fig. 3). In all three cases the passivation removes the states close to the M point from the Fermi level. Therefore, for the passivated surface of HgSe, any possible Dirac point must appear at Γ. However, due to the tiny bulk gap of only several meV, there is a rather long-range hybridization between top and bottom surface states in our slab calculation and the gap at Γ closes rather slowly upon increasing the slab thickness. To obtain a very distinct Dirac cone in HgSe one would need slabs much larger than 12 unit cells, which is beyond the present possibilities of high-precision all-electron methods. Nevertheless, taking into account the results for surface passivation in β-HgS and the similarity of the electronic structures for all investigated X, we see that it is highly likely that the expected Dirac cone will show no large anisotropy for passivated HgSe (001) as well. This statement also holds for the case of HgTe in a situation with a finite bulk band gap, which can be achieved in a calculation by larger strain [33].

We have shown in conclusion that surface termination and decoration can play a crucial role for topological insulators. The topological surface states can be modified with respect to their dispersion, with respect to their spatial location, and, perhaps most importantly, with respect to their anisotropy by using different surface types or by surface decoration. We observe, for example, that surface passivation almost entirely destroys the anisotropy of the Dirac cone of the pure (001) surface of β-HgS and has dramatic consequences for the spin relaxation time τ_S in comparison to the scattering time τ. For the pure surface, an anisotropy of Fermi velocities $v_x/v_y = 18$ leads to the estimate $\tau_S/\tau \approx 10^3$ according to the formulas given in Ref. [14], which can be simplified to $\tau_S/\tau \sim (v_y/v_x)^2$ if the Fermi level coincides with the Dirac point. On the other hand, an isotropic Dirac cone has $\tau_S/\tau = 2$. The notion that anisotropic Fermi velocities are beneficial for the spin-transport properties of TIs suggests that careful surface preparation is needed to keep these desirable properties intact. An intended generation of anisotropy, e.g., by surface decoration, is an idea that still remains to be evidenced.

We thank C. Ortix, K. Koepernik, and M. Ruck for discussion. This work was performed using HPC from GENCI-CINES (Grant No. c2012096873).

*roland.hayn@im2np.fr

[1] C. L. Kane and E. J. Mele, Phys. Rev. Lett. **95**, 146802 (2005).
[2] B. A. Bernevig, T. L. Hughes, and S.-C. Zhang, Science **314**, 1757 (2006).
[3] L. Fu, C. L. Kane, and E. J. Mele, Phys. Rev. Lett. **98**, 106803 (2007).
[4] M. König, S. Wiedmann, C. Brüne, A. Roth, H. Buhmann, L. W. Molenkamp, X.-L. Qi, and S.-C. Zhang, Science **318**, 766 (2007).
[5] D. Hsieh, D. Qian, L. Wray, Y. Xia, Y. S. Hor, R. J. Cava, and M. Z. Hasan, Nature (London) **452**, 970 (2008).
[6] Y. Xia *et al.*, Nat. Phys. **5**, 398 (2009).
[7] C. Wu, B. A. Bernevig, and S.-C. Zhang, Phys. Rev. Lett. **96**, 106401 (2006).
[8] H. Zhang, C.-X. Liu, X.-L. Qi, X. Dai, Z. Fang, and S.-C. Zhang, Nat. Phys. **5**, 438 (2009).
[9] S. Raghu, S. B. Chung, X.-L. Qi, and S.-C. Zhang, Phys. Rev. Lett. **104**, 116401 (2010).
[10] P. Hosur, Phys. Rev. B **83**, 035309 (2011).
[11] J. W. McIver, D. Hsieh, H. Steinberg, P. Jarillo-Herrero, and N. Gedik, Nat. Nanotechnol. **7**, 96 (2011).
[12] A. A. Burkov and D. G. Hawthorn, Phys. Rev. Lett. **105**, 066802 (2010).
[13] P. Schwab, R. Raimondi, and C. Gorini, Europhys. Lett. **93**, 67 004 (2011).
[14] V. E. Sacksteder, S. Kettemann, Q. S. Wu, X. Dai, and Z. Fang, Phys. Rev. B **85**, 205303 (2012).
[15] C. Brüne, C. X. Liu, E. G. Novik, E. M. Hankiewicz, H. Buhmann, Y. L. Chen, X. L. Qi, Z. X. Shen, S. C. Zhang, and L. W. Molenkamp, Phys. Rev. Lett. **106**, 126803 (2011).
[16] A. Svane, N. E. Christensen, M. Cardona, A. N. Chantis, M. van Schilfgaarde, and T. Kotani, Phys. Rev. B **84**, 205205 (2011).
[17] A. Delin, Phys. Rev. B **65**, 153205 (2002).
[18] C.-Y. Moon and S.-H. Wei, Phys. Rev. B **74**, 045205 (2006).
[19] M. Cardona, R. K. Kremer, R. Lauck, G. Siegle, A. Munoz, and A. H. Romero, Phys. Rev. B **80**, 195204 (2009).
[20] R. Sakuma, C. Friedrich, T. Miyake, S. Blügel, and F. Aryasetiawan, Phys. Rev. B **84**, 085144 (2011).
[21] F. Virot, R. Hayn, M. Richter, and J. van den Brink, Phys. Rev. Lett. **106**, 236806 (2011).
[22] K. Koepernik and H. Eschrig, Phys. Rev. B **59**, 1743 (1999); http://www.fplo.de/.
[23] I. Opahle, K. Koepernik, and H. Eschrig, Phys. Rev. B **60**, 14035 (1999).
[24] J. P. Perdew and Y. Wang, Phys. Rev. B **45**, 13244 (1992).
[25] S. Oehling *et al.*, Appl. Phys. Lett. **73**, 3205 (1998).
[26] D. Eich, D. Hubner, K. Ortner, L. Kilian, R. Becker, G. Landwehr, R. Fink, and E. Umbach, Appl. Surf. Sci. **166**, 12 (2000).
[27] F. Virot, Ph.D. thesis, University Aix-Marseille, Marseille, France, 2012.
[28] F. Tinjoux, Ph.D. thesis, University Joseph Fourier, Grenoble, France, 2003.
[29] C. Bouvier, T. Meunier, R. Kramer, and L. P. Lévy, arXiv:1112.2092.
[30] G. Debias, J. Barcelo, J. P. Aicardi, G. Masse, and F. Bombre, Thin Solid Films **7**, 11 (1971).
[31] G. W. Bryant, Phys. Rev. B **35**, 5547 (1987).
[32] J. T. Schick, S. M. Bose, and A.-B. Chen, Phys. Rev. B **40**, 7825 (1989).
[33] B. Yan and S.-C. Zhang, Rep. Prog. Phys. **75**, 096501 (2012).